

THE POPULATION OF DAMPED LYMAN-ALPHA AND LYMAN LIMIT SYSTEMS IN THE COLD DARK MATTER MODEL

Jeffrey P. Gardner¹, Neal Katz¹, Lars Hernquist^{2,3}, David H. Weinberg⁴

E-mail: gardner@astro.washington.edu, nsk@astro.washington.edu, lars@ucolick.org,
dhw@payne.mps.ohio-state.edu

ABSTRACT

Lyman limit and damped Ly α absorption systems probe the distribution of collapsed, cold gas at high redshift. Numerical simulations that incorporate gravity and gas dynamics can predict the abundance of such absorbers in cosmological models. We develop a semi-analytical method to correct the numerical predictions for the contribution of unresolved low mass halos, and we apply this method to the Katz et al. (1996) simulation of the standard cold dark matter model ($\Omega = 1$, $h = 0.5$, $\Omega_b = 0.05$, $\sigma_8 = 0.7$). Using this simulation and higher resolution simulations of individual low mass systems, we determine the relation between a halo's circular velocity v_c and its cross section for producing Lyman limit or damped Ly α absorption. We combine this relation with the Press-Schechter formula for the abundance of halos — itself calibrated against the simulated halo population — to compute the number of absorbers per unit redshift. The resolution correction increases the predicted abundances by about a factor of two at $z = 2$, 3 , and 4 , bringing the predicted number of damped Ly α absorbers into quite good agreement with observations. Roughly half of these systems reside in halos with circular velocities $v_c \geq 100 \text{ km s}^{-1}$ and half in halos with $35 \text{ km s}^{-1} \leq v_c \leq 100 \text{ km s}^{-1}$. Halos with $v_c > 150 \text{ km s}^{-1}$ typically harbor two or more systems capable of producing damped absorption. Even with the resolution correction, the predicted abundance of Lyman limit systems is a factor of three below observational estimates, signifying either a failure of the standard cold dark matter model or a failure of these simulations to resolve most of the systems responsible for Lyman limit absorption. By comparing simulations with and without star formation, we find that depletion of the gas supply by star formation affects absorption line statistics at $z \geq 2$ only for column densities exceeding $N_{\text{HI}} = 10^{22} \text{ cm}^{-2}$, even though half of the cold, collapsed gas has been converted to stars by $z = 2$.

¹University of Washington, Department of Astronomy, Seattle, WA 98195

²University of California, Lick Observatory, Santa Cruz, CA 95064

³Presidential Faculty Fellow

⁴Ohio State University, Department of Astronomy, Columbus, OH 43210

Subject headings: quasars: absorption lines, galaxies: formation, large-scale structure of the Universe

1. Introduction

Systems producing absorption in the spectra of distant quasars offer an excellent probe of the early Universe. At high redshifts, they easily outnumber other observed tracers of cosmic structure, including both normal and active galaxies. Mounting evidence that the high column density absorbers are young galaxies links relatively pristine baryonic matter to highly evolved objects at the present day. The amount of atomic hydrogen in damped Ly α (DLA) absorbers at $z \sim 3$ is comparable to the mass in stars at the current epoch (Wolfe 1988), and two DLA systems are known to have radial extents $\gtrsim 10h^{-1}$ kpc (Briggs et al. 1989; Wolfe et al. 1993). Photometry of damped absorbers supports the view that they are high-redshift galaxies (Djorgovski et al. 1996; Fontana et al. 1996). At somewhat lower column densities and redshifts, deep imaging and spectroscopy indicate that Lyman limit systems are associated with lines of sight passing near bright galaxies (Yanny 1990; Lanzetta & Bowen 1990; Bergeron & Boissé 1991; Steidel, Dickinson, & Persson 1994) or galaxy clusters (Lanzetta, Webb, & Barcons 1996).

The interpretation of quasar absorption systems has undergone something of a revolution during the past two years, with the recognition that they may be gas aggregating into nonlinear structures in hierarchical models like those invoked to account for the observed galaxy distribution (e.g., Cen et al. 1994; Petitjean, Mucket, & Kates 1995; Zhang, Anninos, & Norman 1995; Hernquist et al. 1996; Miralda-Escudé et al. 1996). In particular, Katz et al. (1996; hereafter KWHM) used simulations that evolve baryons and dark matter in the presence of a background radiation field to show that high column density absorbers arise naturally in a cold dark matter (CDM) universe from radiatively cooled gas in galaxy-sized halos, supporting the notion that damped Ly α systems are a byproduct of galaxy formation. Together with the results of Hernquist et al. (1996) for the Ly α forest, the column density distribution predicted by KWHM matches existing data reasonably well, but it falls below the observations by factors ≈ 2 and ≈ 8 for DLA and Lyman limit absorbers, respectively.

This discrepancy can be attributed at least partly to resolution effects in the simulations. Owing to computational expense, the KWHM simulation could not resolve halos with circular velocities below $v_c \approx 100$ km s $^{-1}$. However, higher resolution simulations of localized regions by Quinn, Katz, & Efstathiou (1996; hereafter QKE) indicate that halos down to $v_c \approx 35$ km s $^{-1}$ can host damped absorbers, so clearly the number of high column density systems found by KWHM is artificially depressed by the finite resolution of their simulation.

In this paper, we overcome this numerical limitation using a two-step correction procedure. First, we employ the Press & Schechter (1974) algorithm to correct the KWHM data by extending

the halo mass function to values lower than could be resolved by their simulation. Then, we account for absorption by gas in these halos from a relation between the absorption cross section for a halo and its circular velocity. This relation is established by fitting both the KWHM data and high-resolution simulations that use the QKE initial conditions and the KWHM background radiation field. These additional simulations examine localized regions around low mass objects with sufficient resolution to resolve halos down to $v_c \approx 35 \text{ km s}^{-1}$. Heating by the UV background prevents the collapse and cooling of gas in smaller halos (QKE; Thoul & Weinberg 1996). The high-resolution volumes are small and were chosen in a non-random way, so they cannot be used directly to infer the number of DLA and Lyman limit systems. By convolving the absorption area vs. circular velocity relation with the halo mass function given by the Press-Schechter method, we can predict the absorption at any mass scale, effectively extending the dynamic range of the simulations down to the lowest mass objects that produce high column density absorption. We also present another calculation, similar to that in KWHM but including star formation, to quantify the effects of gas depletion on high column density absorption.

2. Simulations and Methods

Our primary simulation, the same as that used by KWHM, follows the evolution of a periodic cube whose edges measure 22.22 Mpc in comoving units. This region was drawn randomly from a CDM universe with $\Omega = 1$, $h \equiv H_0/100 \text{ km s}^{-1} \text{ Mpc}^{-1} = 0.5$, baryon density $\Omega_b = 0.05$, and power spectrum normalization $\sigma_8 = 0.7$. A uniform background radiation field was imposed to mimic the expected ultraviolet (UV) output of quasars, with a spectrum of the form $J(\nu) = J_0(\nu_0/\nu)F(z)$, where ν_0 is the Lyman-limit frequency, $J_0 = 10^{-22} \text{ erg s}^{-1} \text{ cm}^{-2} \text{ sr}^{-1} \text{ Hz}^{-1}$, and $F(z) = 0$ if $z > 6$, $F(z) = 4/(1+z)$ if $3 \leq z \leq 6$, and $F(z) = 1$ if $2 < z < 3$. The simulations employ 64^3 gas and 64^3 dark-matter particles, with a gravitational softening length of 20 comoving kpc (13 comoving kpc equivalent Plummer softening). The particle mass is $1.45 \times 10^8 M_\odot$ and $2.8 \times 10^9 M_\odot$ for gas and dark matter, respectively. Detailed descriptions of the simulation code and the radiation physics can be found in Hernquist & Katz (1989) and Katz, Weinberg, & Hernquist (1996; hereafter KWH). The low column density absorption in this simulation is discussed by Hernquist et al. (1996), and the galaxy population is discussed by Weinberg, Hernquist, & Katz (1996).

We also employ two simulations that have the same initial conditions, cosmological parameters, and numerical parameters as QKE but the UV background spectrum given above. These comprise smaller, 10 Mpc periodic volumes (with $\Omega = 1$, $h = 0.5$, $\Omega_b = 0.05$ as before), which are evolved using a hierarchical grid of particles in the initial conditions. The central region forms a collapsed object that is represented using a large number of low mass particles, while regions further away are modeled using a small number of more massive particles. A simulation of the same volume as QKE would require 256^3 particles of each species to match the resolution of the central region throughout; the nesting technique allows us to achieve high-resolution locally while preserving the

cosmological context of the calculation.

QKE find that a photoionizing background suppresses the collapse and cooling of gas in halos with circular velocities $v_c \lesssim 35 \text{ km s}^{-1}$. Thoul & Weinberg (1996) find a similar cutoff in much higher resolution, spherically symmetric calculations. Hence, it should be possible to estimate the amount of gas capable of producing DLA and Lyman limit absorption by accounting for halos down to this cutoff in v_c . Both QKE and Thoul & Weinberg (1996) find that photoionization has little effect on the amount of gas that cools in halos with $v_c \gtrsim 60 \text{ km s}^{-1}$, consistent with the results of Navarro & Steinmetz (1996) and Weinberg et al. (1996).

The current generation of hydrodynamic simulations lacks the dynamic range necessary to represent halos over the entire range $35 < v_c \lesssim 300 \text{ km s}^{-1}$. To overcome this limitation, we use the approximation developed by Press & Schechter (1974), who give the following analytic estimate for the number density of halos of mass M at redshift z :

$$N(M, z) dM = \sqrt{\frac{2}{\pi}} \frac{\rho_0}{M} \frac{\delta_c}{\sigma_0} \left(\frac{\gamma R_f}{R_*} \right)^2 \exp \left(\frac{-\delta_c^2}{2\sigma_0^2} \right) dM, \quad (1)$$

where ρ_0 is the mean comoving density, R_f is the Gaussian filter radius corresponding to mass $M = (2\pi)^{3/2} \rho_0 R_f^3$, and δ_c is the critical linear density contrast that corresponds to gravitational collapse. The parameters σ_0 , γ and R_* are related to moments of the power spectrum (Bardeen et al. 1986). Equation (1) can be integrated from M to infinity to yield the number density of objects above a given mass. In what follows, for comparison with our simulations, we use the CDM transfer function given by Bardeen et al. (1986).

To determine the number of DLA and Lyman limit systems per unit redshift, we first fix the parameters in the Press-Schechter algorithm so that it reproduces the mass function of our 22.22 Mpc simulations. Then, we use the 22.22 Mpc and 10 Mpc simulations together to fit a relation between the circular velocity of a halo and its cross section for producing DLA or Lyman limit absorption.

To identify halos in the simulations, we apply a friends-of-friends algorithm with a linking length equal to the mean interparticle separation on an isodensity contour of an isothermal sphere with an overdensity 177, $b = (177n/3)^{-1/3}$ where n is the particle number density. We also apply the algorithm of Stadel et al. (1996; see also KWH and <http://www-hpcc.astro.washington.edu/tools/DENMAX>) to the cold gas particles in the same volume to locate regions of collapsed gas capable of producing Lyman limit and damped Ly α absorption. A region of gas is considered a potential absorber only if it contains at least four gas particles that are mutually bound, have a smoothed overdensity $\rho_g/\bar{\rho}_g > 170$, and a temperature $T < 30,000 \text{ K}$. All of the gas concentrations found by this method are associated with a friends-of-friends halo, even at $z = 4$. We match each absorber with its parent halo and discard halos that contain no absorbers.

For each of the halos that contains a cold gas concentration, we determine the radius of the sphere centered on the most tightly bound particle within which the average density is equal to

177 times the mean background density. We characterize halo masses and circular velocities by their values at this radius. This method of quantifying the properties of halos in the simulations corresponds to that envisioned in the Press-Schechter approximation, which is based on the spherical collapse model. We find that the mass distribution of halos in the simulations is best fit using the Press-Schechter form with a Gaussian filter and $\delta_c = 1.69$. Many workers have instead used a top-hat filter, with $M_f = (4\pi/3)\rho_0 R_f^3$ (*cf.* Ma 1996; Ma & Bertschinger 1994; Mo & Miralda-Escudé 1994; Mo et al. 1996), or a Gaussian filter with a modified relation between filter radius and associated mass, $M_f = 6\pi^2\rho_0 R_f^3$ (Lacey & Cole 1994), with similar values for δ_c . However, these studies used the halo masses as returned by the friends-of-friends algorithm itself, and if we do this we also find that top-hat or modified Gaussian filters provide good fits to the mass function for $\delta_c \approx 1.7$. The combination $\delta_c = 1.69$, Gaussian filter, and $M_f = (2\pi)^{3/2}\rho_0 R_f^3$ is appropriate for our definition of halo masses within overdensity 177 spheres. Including or excluding the “absorberless” halos in our mass function does not change the results above $v_c = 100$ km s^{−1} because all halos above this circular velocity contain at least one absorber.

We calculate HI column densities for the halos by encompassing each halo with a sphere which is centered on the most tightly bound gas particle and is of a sufficient size to contain all gas particles which may contribute to absorption within the halo. We project the gas distribution within this sphere onto a uniform grid of cell size 5.43 comoving kpc, equal to the highest resolution achieved anywhere in the 22.22 Mpc simulation. Using the method of KWHM, we calculate an initial HI column density for each gridpoint assuming that the gas is optically thin, then apply a self-shielding correction to yield a true HI column density (see KWHM for details). For each halo we compute the projected area over which it produces damped absorption, with $N_{\text{HI}} > 10^{20.3}$ cm^{−2}, and Lyman limit absorption, with $N_{\text{HI}} > 10^{17.2}$ cm^{−2}. For simplicity, we project all halos from a single direction, though we obtain a similar fit of absorption area to circular velocity if we project randomly in the x , y , and z directions or average the projections in x , y , and z .

Figure 1 shows the cross section for damped absorption (left hand panels) and Lyman limit absorption (right hand panels) as a function of circular velocity for each of our halos, at redshifts 2, 3, and 4. The open circles at low v_c represent halos from the 10 Mpc, high-resolution runs. Other points refer to the 22.22 Mpc simulation, and the number of vertices in each symbol indicates the number of absorbers (*i.e.*, distinct regions of cold, collapsed gas) within each halo. For these halos there are two competing effects that determine the trend between absorption cross section and circular velocity. Higher mass halos have deeper potential wells, so concentrations of cold gas contract further, explaining the downward trend in cross section with circular velocity exhibited by points with a fixed number of vertices. However, more massive halos tend to harbor more than one concentration of gas, increasing their absorption cross section. The overall trend in Figure 1 is that halos of higher circular velocities on average have larger absorption cross sections.

The solid lines in Figure 1 show a smooth function $\alpha_z(v_c)$ fitted to the relation between absorption area and circular velocity. We will need this function for our Press-Schechter correction

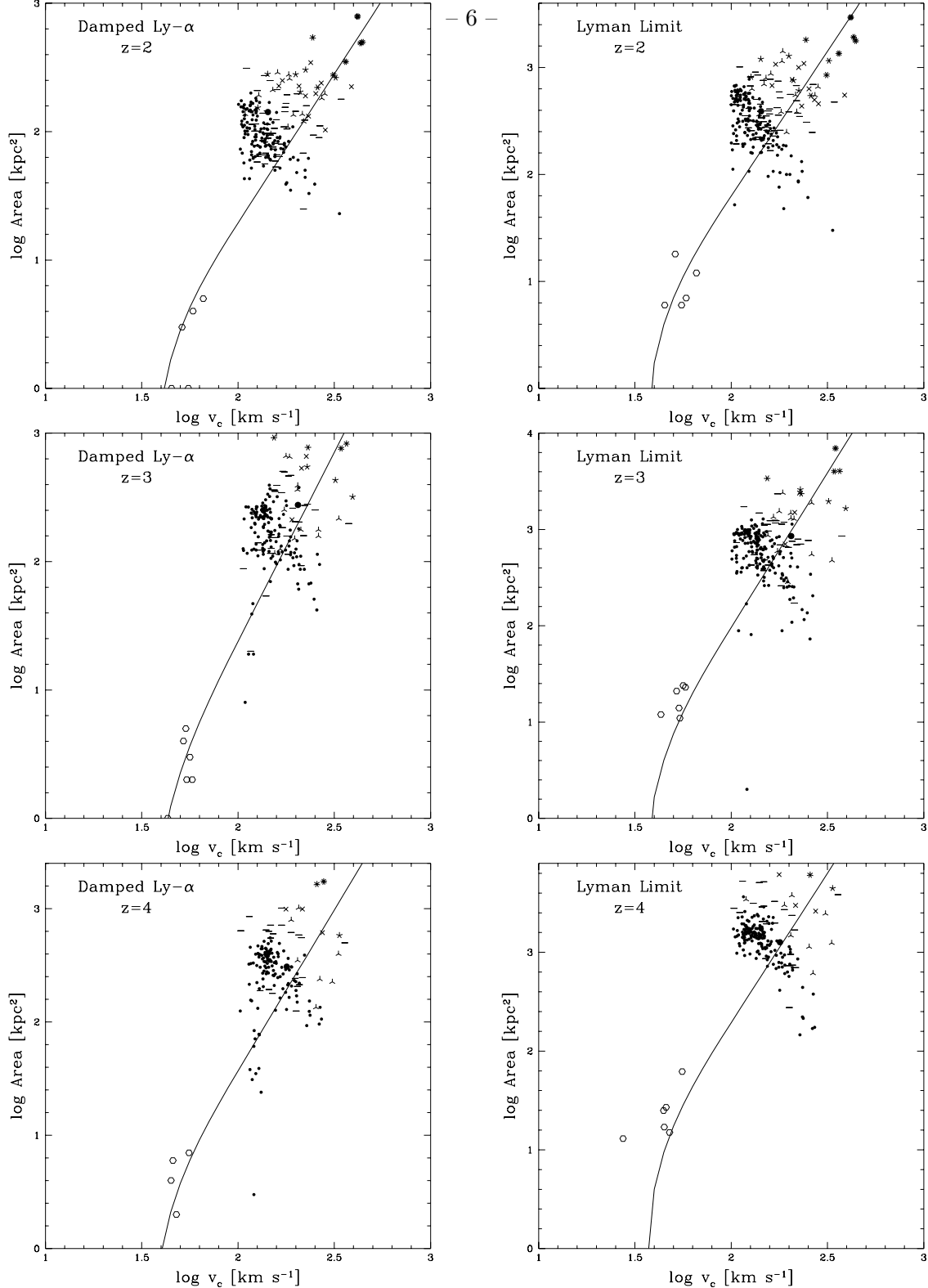


Fig. 1.— Comoving absorbing area in kpc^2 vs. circular velocity v_c in km s^{-1} for halos in the 22.22 Mpc simulation (skeletal points) and the 10 Mpc simulations (open circles). Left hand panels show the area for DLA absorption, $N_{\text{HI}} \geq 10^{20.3} \text{ cm}^{-2}$, and right hand panels for Lyman limit absorption, $N_{\text{HI}} \geq 10^{17.2} \text{ cm}^{-2}$. The number of vertices in the skeletal points corresponds to the number of gas concentrations in the halo. The solid line shows the fitted smooth relation of equation (2), with parameter values listed in Table 1.

procedure below. As a functional form we adopt a linear relation between $\log \alpha$ and $\log v_c$ with a damping factor $1 - \exp(-(v_c - 35)/12)$, which reflects the suppression of gas cooling in low v_c halos. We bin the data points in intervals of 0.15 in $\log v_c$, compute the mean and standard deviation of $\log \alpha$ in each bin, and determine the parameters of the smooth relation by χ^2 minimization. Fitting binned data rather than individual halos gives more appropriate weight to the relatively rare, high v_c halos. Table 1 lists the fitted values of A and B for the functional relation

$$\log \alpha = (A \log v_c + B)(1 - \exp(-(v_c - 35)/12)), \quad (2)$$

with α in comoving kpc^2 , v_c in km s^{-1} , and base-10 logarithms. We determine values separately for DLA and Lyman limit absorption and for each redshift. Figure 1 shows that there is substantial scatter about this mean relation, and our adopted functional form is rather arbitrary, but we will see shortly that this characterization of the $\alpha_z(v_c)$ relation suffices for our purposes.

The observable quantity that we would like to test the CDM model against is $n(z)$, the number of DLA or Lyman limit absorbers per unit redshift interval along a random line of sight. We can estimate this from the projected HI map of the 22.22 Mpc simulation as in KWHM, by dividing the fractional area that has projected column density above the DLA or Lyman limit threshold by the depth of the box in redshift. However, because the simulation does not resolve gas cooling in halos with $v_c \lesssim 100 \text{ km s}^{-1}$, this procedure really yields estimates of $n(z, 100 \text{ km s}^{-1})$, where $n(z, v_c)$ denotes the number of absorbers per unit redshift produced by halos with circular velocity greater than v_c . Since halos with $35 \text{ km s}^{-1} < v_c < 100 \text{ km s}^{-1}$ can harbor DLA and Lyman limit absorbers, $n(z, 100 \text{ km s}^{-1})$ is only a lower limit to the observable quantity $n(z)$.

We have now assembled the tools to fix this problem, for the Press-Schechter formula (1) tells us the number density of halos as a function of circular velocity and the relation $\alpha_z(v_c)$ tells us how much absorption these halos produce. Equation (1) is given in terms of the mass M ; since we define the halo mass within a sphere of overdensity 177, the corresponding circular velocity is

$$v_c = (GM/R_{177})^{1/2} = \left[GM^{2/3} \left(\frac{4\pi}{3} 177 \rho_c \right)^{1/3} \right]^{1/2} = 117 \left(\frac{M}{10^{11} M_\odot} \right)^{1/3} \left(\frac{1+z}{4} \right)^{1/2} \text{ km s}^{-1}. \quad (3)$$

Thus,

$$n(z, v_c) = \frac{dr}{dz} \int_M^\infty N(M', z) \alpha_z(v_c) dM', \quad (4)$$

where $N(M', z)$ is taken from equation (1), and equation (3) is used to convert between v_c and M as necessary. Multiplying the comoving number density of halos by the comoving absorption area

z	A_{DLA}	B_{DLA}	B_{LL}	B_{LL}
2.0	2.32	-1.87	2.70	-2.13
3.0	2.94	-3.03	3.21	-2.96
4.0	2.84	-2.63	3.02	-2.28

Table 1: Fitted parameter values for $\alpha_z(v_c)$, with the functional form in equation (2).

yields a number of absorbers per comoving distance, and multiplying by dr/dz , the derivative of comoving distance with respect to redshift, converts to a number per unit redshift.

Figure 2 shows $n(z, v_c)$ computed from equation (4) using our fitted relations $\alpha_z(v_c)$. Starting from high v_c , the abundance first rises steeply with decreasing v_c because of the increasing number of halos, but it flattens at low v_c because of the suppression of gas cooling in small halos. Points with error bars show $n(z, v_c)$ obtained directly from the halos in the 22.22 Mpc simulation. The curves fit these points quite well — they are, of course, constructed to do so, but the agreement shows that our full procedure, including the details of the Press-Schechter calibration and fitting for $\alpha_z(v_c)$, is able to reproduce the original numerical results in the regime where halos are resolved. We can therefore be fairly confident in using this method to extrapolate to $n(z, 0) = n(z)$, the incidence of high column density absorption produced by gas in all halos, thus incorporating the new information provided by the high-resolution simulations. These values of $n(z)$, the y -intercepts of the curves in the panels of Figure 2, are the principal numerical results of this paper. We will compare them to observations in the next section.

Table 2 lists the values of $n(z)$ determined by this procedure at $z = 2, 3$, and 4 . It also lists the correction factors that must be applied to the quantities $n(z, 100 \text{ km s}^{-1})$ obtainable by the KWHM procedure in order to get the total abundance $n(z) = n(z, 0)$. In all cases, roughly half of the absorption occurs in halos with $v_c > 100 \text{ km s}^{-1}$ and half in the more common but smaller halos with lower circular velocities.

3. Comparison to Observations

Figure 3 compares our derived values of $n(z)$ to observational estimates of the incidence of damped Ly α absorption, taken from Storrie-Lombardi et al. (1996) and Wolfe et al. (1995), and Lyman limit absorption, taken from Storrie-Lombardi et al. (1994). The theoretical predictions and observed values are listed in Table 2. The resolution correction increases the predicted $n(z)$ values relative to those of KWHM by about a factor of two, leading to quite good agreement with the observed abundance of DLA absorbers at $z = 2$ and 3 . At $z = 4$ the predicted abundance is 1.6σ below the Storrie-Lombardi et al. (1996) data. Since there are systematic as well as statistical uncertainties in this observational estimate — in particular, it includes candidate DLA systems that have not yet been confirmed by Echelle spectroscopy — we regard this level of agreement as acceptable.

The situation for Lyman limit absorption is quite different. Here the theoretical predictions fall systematically below the observed abundances, by about a factor of three. The correction for unresolved halos reduces the discrepancy found by KWHM, but it does not remove it. The deficit of Lyman limit systems could reflect a failing of the CDM model considered here, or it could indicate the presence in the real universe of an additional population of Lyman limit absorbers

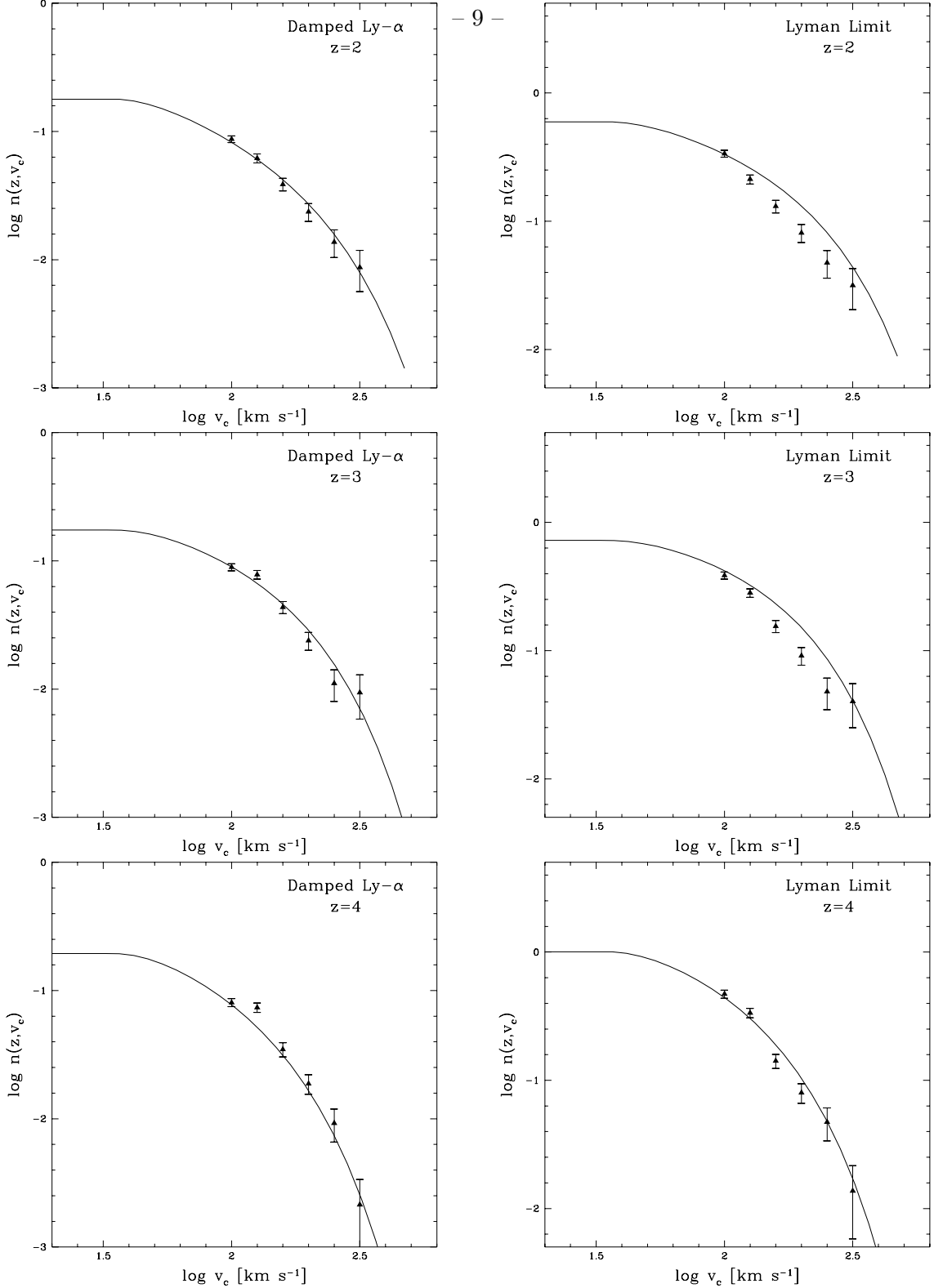


Fig. 2.— Incidence of DLA (left) and Lyman limit (right) absorption at $z = 2, 3$, and 4 . Curves show $n(z, v_c)$, the number of absorbers per unit redshift arising in halos with circular velocity greater than v_c , computed from equation (4). The y -intercepts show the incidence of absorption produced by all halos. Points with $N^{1/2}$ error bars show numerical results from the 22.22 Mpc simulation.

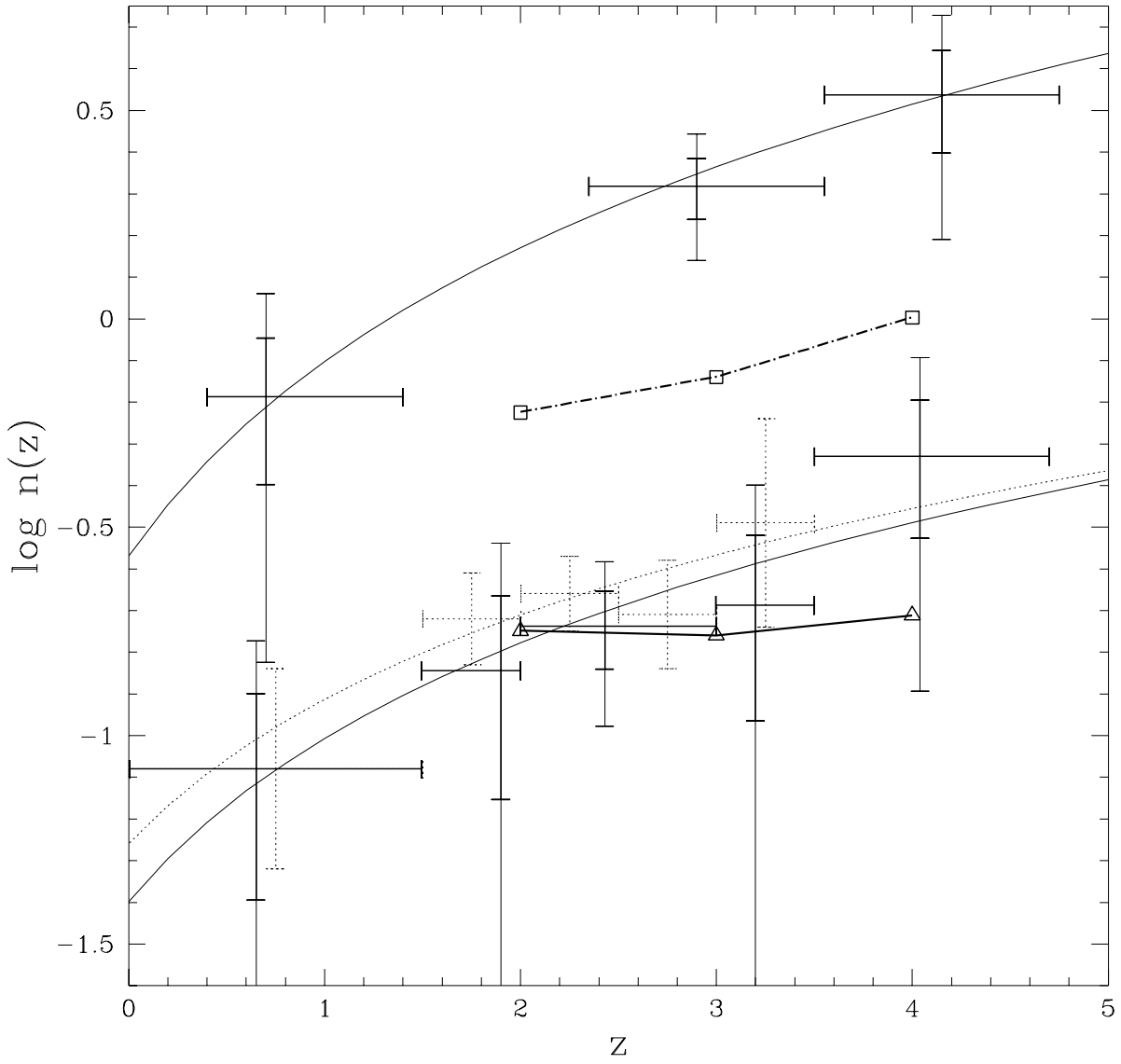


Fig. 3.— Incidence of DLA and Lyman limit absorption as a function of redshift. Triangles and squares show the resolution-corrected theoretical predictions for DLA and Lyman limit absorption, respectively. The upper error crosses represent the Lyman limit data of Storrie-Lombardi et al. (1994), with 1σ and 2σ abundance errors shown. The smooth curve shows their fitted power law. The lower set of error crosses and solid curve represent the DLA data of Storrie-Lombardi et al. (1996), with 1σ and 2σ errors. The dotted error crosses and curve show the data, 1σ errors, and fit from Wolfe et al. (1995).

that are not resolved by our simulations. We discuss this issue further in § 5.

4. Effects of Star Formation

The simulations examined in the previous section do not allow conversion of gas into stars, and one might worry that depletion of the atomic gas supply by star formation would substantially reduce the predicted abundance of DLA absorbers. We investigate this issue by analyzing a simulation identical to the KWHM run considered above except that it incorporates star formation. The algorithm, a modified form of that introduced by Katz (1992), is described in detail by KWH; we summarize it here. A gas particle becomes “eligible” to form stars if (a) the local hydrogen density exceeds 0.1 cm^{-3} (similar to that of neutral hydrogen clouds in the interstellar medium), (b) the local overdensity exceeds the virial overdensity, and (c) the particle resides in a converging flow that is Jeans-unstable. Star formation takes place gradually, with a star formation rate that depends on an assumed efficiency for conversion of gas into stars and on the local collapse timescale (the maximum of the local dynamical timescale and the local cooling timescale). We set the efficiency parameter defined by KWH to $c_* = 0.1$, though the tests in KWH show that results are insensitive to an order-of-magnitude change in c_* . Until the gas mass of such a particle falls below 5% of its original mass, it is categorized as a “star-gas” particle. Thereafter, it is treated as a collisionless star particle. This gradual transition overcomes computational difficulties associated with alternative implementations of star formation, such as the artificial reduction in resolution caused by rapid removal of collisionless gas particles from converging flows, or the spawning of a large number of extra particles that slow the computations and consume memory.

When stars form, we add supernova feedback energy to the surrounding gas in the form of heat, assuming that each supernova yields 10^{51} ergs and that all stars greater than $8M_\odot$ go supernova. We add this energy gradually, with an exponential decay time of 2×10^7 years, the approximate lifetime of an $8M_\odot$ star. Thermal energy deposited in the dense, rapidly cooling gas is quickly radiated away, so although feedback has some effect in our simulation, the impact is usually not dramatic.

Figure 4 shows column density distributions for the simulations with and without star formation at $z = 2, 3$, and 4 ; $f(N_{\text{HI}})$ is the number of absorbers per unit redshift per linear interval of column density. Star formation alters $f(N_{\text{HI}})$ only at column densities greater than 10^{22} cm^{-2} , higher than any observed column density. Star formation does affect the amount of cold, collapsed gas, however. The simulation without star formation yields an Ω in cold, collapsed gas, i.e. gas with $\rho/\bar{\rho} > 1000$ and $T < 30,000 \text{ K}$, of $(6.5, 3.6, 1.7) \times 10^{-3}$ at $z = (2, 3, 4)$. In the simulation with star formation, the Ω in cold, collapsed gas is $(3.4, 2.3, 1.2) \times 10^{-3}$ at $z = (2, 3, 4)$, while the Ω in stars is $(3.1, 1.2, 0.4) \times 10^{-3}$, making a total Ω in collapsed galactic baryons of $(6.5, 3.5, 1.6) \times 10^{-3}$, just slightly below the simulation without star formation. Hence, star formation simply converts

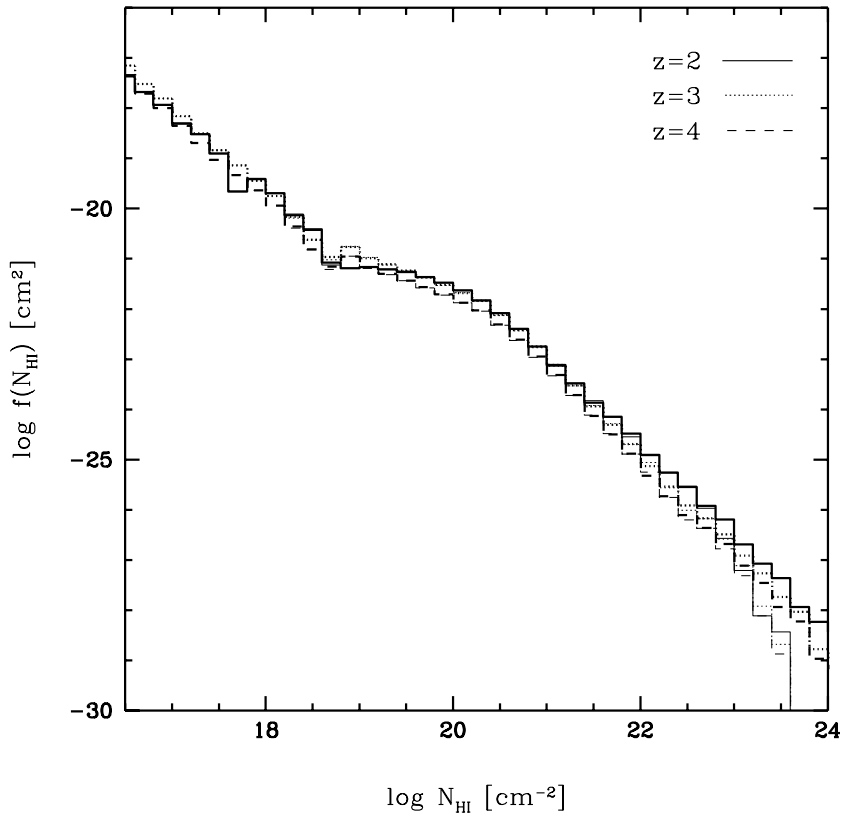


Fig. 4.— The column density distribution $f(N_{\text{HI}})$ — the number of absorbers per unit redshift per linear interval of N_{HI} — for simulations with and without star formation. Histograms show the simulation results at $z = 2$ (solid), $z = 3$ (dotted), and $z = 4$ (dashed). Heavier lines represent the simulation without star formation and lighter lines the simulation with star formation.

very high column density gas into stars while affecting little else. It does not significantly alter the predicted values of $n(z)$ given previously because absorbers with $N_{\text{HI}} \geq 10^{22} \text{ cm}^{-2}$ are a small fraction of all DLA absorbers.

All of the distributions in Figure 4 show a clear flattening in the column density range $10^{18.5} \text{ cm}^{-2} \leq N_{\text{HI}} \leq 10^{20.5} \text{ cm}^{-2}$. This flattening reflects the onset of self-shielding. A small range of total hydrogen column densities maps into a wider range of neutral hydrogen column densities because the neutral fraction rises rapidly with column density as self-shielding becomes important. While the optical depth to Lyman limit photons is one at $N_{\text{HI}} = 10^{17.2} \text{ cm}^{-2}$, self-shielding does not become strong until significantly higher column densities because higher frequency photons have a lower ionization cross section and can still penetrate the cloud.

5. Summary

The finite resolution of numerical simulations affects their predictions for the abundance $n(z)$ of DLA and Lyman limit absorption systems. It is not currently feasible to simulate a volume large enough to contain a representative population of high circular velocity halos while maintaining enough resolution to accurately model the smallest halos ($v_c \approx 35 \text{ km s}^{-1}$) that can harbor such systems. We have therefore devised a method that integrates results from high- and low-resolution simulations to obtain accurate predictions for $n(z)$. We use the simulations to determine the relation between absorption cross section and halo circular velocity over the full range of relevant circular velocities, then combine this relation with the Press-Schechter formula for halo abundance — itself calibrated against the simulated halo population — to compute $n(z)$ via equation (4).

As a method to correct for finite resolution, this technique should be quite reliable, and it can be applied to other cosmological models once the appropriate simulations are available for calibrating $\alpha_z(v_c)$. In the absence of these simulations, one can make the plausible but uncertain assumption that the relation between absorbing area and halo circular velocity is similar from one model to another, then combine $\alpha_z(v_c)$ from this study with the Press-Schechter halo abundance for other models to predict $n(z)$. We apply this approach to a number of popular cosmological scenarios in a separate paper (Gardner et al. 1996). While it is less secure than the resolution-corrected numerical approach of this paper, it is an improvement over existing semi-analytic calculations of DLA abundances (e.g., Mo & Miralda-Escudé 1994; Kauffmann & Charlot 1994; Ma & Bertschinger 1994; Klypin et al. 1995), which usually assume that *all* gas within the halo virial radius cools and becomes neutral, and which either assume a form and scale for the collapsed gas distribution or compare to observations only through the atomic gas density parameter Ω_g , which is sensitive mainly to the very highest column density systems.

Our resolution correction increases the incidence of DLA and Lyman limit absorption in the CDM model by about a factor of two, relative to the results of KWHM. This increase brings the

predicted abundance of DLA absorbers into quite good agreement with observations at $z = 2$ and 3, indicating that the high redshift galaxies that form in the CDM model can account naturally for the observed damped Ly α absorption. At $z = 4$ the predicted $n(z)$ is 1.6σ (a factor 2.4) below a recent observational estimate. However, many of the systems that contribute to this data point have not yet been confirmed by high-resolution spectroscopy, so the estimate may decrease with future observations.

The underprediction of Lyman limit absorption in the simulations is more dramatic, nearly a factor of three at $z = 2, 3$, and 4. This discrepancy could represent a failure of the CDM model with our adopted parameters ($\Omega = 1, h = 0.5, \Omega_b = 0.05, \sigma_8 = 0.7$), though most of the popular alternatives to standard CDM have less small scale power and therefore fare at least as badly in this regard. An alternative possibility is that most Lyman limit absorption occurs in structures far below the resolution scale of even our high-resolution, individual object simulations. For example, Mo & Miralda-Escudé (1996) propose that most Lyman limit systems are low mass ($\sim 10^5 M_\odot$) clouds formed by thermal instabilities in galactic halo gas. We could also be underestimating Lyman limit absorption if some of it arises in partially collapsed structures — sheets or filaments — that are not accounted for by the Press-Schechter halo formula. While the KWHM simulation includes such structures, it may underestimate their numbers in regions of low background density, where its spatial resolution is degraded, and the QKE simulations select high density regions from the outset. High resolution simulations focused on underdense regions could investigate this possibility. At lower redshifts Lyman limit absorption is always associated with normal galaxies (Steidel et al. 1994; Lanzetta et al. 1996), but this is not necessarily the case at high redshifts.

In addition to resolution-corrected estimates of $n(z)$, our results provide some insights into the physical nature of DLA absorbers. As shown in Figure 2, roughly half of the absorbers reside in halos with circular velocities greater than 100 km s^{-1} and half in halos with $35 \text{ km s}^{-1} \leq v_c \leq 100 \text{ km s}^{-1}$. High resolution spectroscopy of metal-line absorption in damped systems (e.g., Wolfe et al. 1994) may be able to test this prediction over the next few years, and future simulations can provide predictions for other cosmological models. We find that halos with $v_c \geq 150 \text{ km s}^{-1}$ frequently host more than one gas concentration (Figure 1), so imaging observations might often reveal multiple objects close to the line of sight.

At $z \geq 2$, star formation and feedback — at least as implemented in our simulations — have virtually no effect on the predicted numbers of Lyman limit and DLA absorbers. Roughly half of the cold, collapsed gas is converted to stars by $z = 2$, but this affects the absorption statistics only at $N_{\text{HI}} \geq 10^{22} \text{ cm}^{-2}$. Depletion of the gas supply by star formation may account for the absence of observed systems with column densities in this range, though the number expected in existing surveys would be small in any case. At lower redshifts, the effects of gas depletion may extend to lower column densities. For $\Omega = 1$ and $h = 0.5$, there are just over a billion years between $z = 4$ and $z = 2$, but there are over two billion years between $z = 2$ and $z = 1$ and over eight billion years from $z = 1$ to the present. Assuming a roughly constant star formation rate in disk galaxies, most of the depletion of DLA gas would occur at low redshifts.

Ongoing searches for DLA absorbers are improving the observational constraints on their abundance at high redshift, and follow-up spectroscopic studies of their metal-line absorption and imaging studies of associated Ly α and continuum emission are beginning to yield important insights into their physical properties. Multi-color searches for “Lyman-break” galaxies are beginning to reveal the population of “normal” high redshift galaxies, which are the likely sources of most DLA absorption. In the hierarchical clustering framework, the abundance, properties, and clustering of these objects depend on the amount of power in the primordial fluctuation spectrum on galactic mass scales, which in turn depends on the nature of dark matter, on the mechanism that produces the fluctuations, and on cosmological parameters such as Ω , h , and Ω_b . The initial fluctuations on galactic scales are difficult to constrain with local observations because much larger structures (e.g., galaxy clusters) have since collapsed. The comparison between rapidly improving high redshift data and numerical simulations like those used here opens a new window for testing cosmological models, and we expect that it will take us much further towards understanding the origin of quasar absorbers, high redshift galaxies, and the galaxies that we observe today.

This work was supported in part by the San Diego, Pittsburgh, and Illinois supercomputer centers, the Alfred P. Sloan Foundation, NASA Theory Grants NAGW-2422, NAGW-2523, NAG5-2882, and NAG5-3111, NASA HPCC/ESS Grant NAG5-2213, NASA grant NAG5-1618, and the NSF under Grant ASC 93-18185 and the Presidential Faculty Fellows Program.

REFERENCES

Bardeen, J. M., Bond, J. R., Kaiser, N., & Szalay, A. S. 1986, ApJ, 304, 15
Bergeron, J., & Boissé, P. 1991, A&A, 243, 344
Briggs, F. H., Wolfe, A. M., Liszt, H. S., Davis, M. M., & Turner, K. L. 1989, ApJ, 341, 650
Cen, R., Miralda-Escudé, J., Ostriker, J. P., & Rauch, M. 1994, ApJ, 437, L9
Djorgovski, S. G., Pahre, M. A., Bechtold, J., & Elston, R. 1996, in press, (astro-ph 9605154)
Fontana, A., Cristiani, S., D’Odorico, S., Giallongo, E., & Savaglio, S. 1996, MNRAS, in press, (astro-ph 9601086)
Gardner, J. P., Katz, N., Weinberg, D. H., & Hernquist, L. 1996, in preparation
Hernquist, L., & Katz, N. 1989, ApJS, 70, 419
Hernquist, L., Katz, N., Weinberg, D. H., & Miralda-Escudé, J. 1996, ApJ, 457, L51
Katz, N. 1992, ApJ, 391, 502
Katz, N., Weinberg, D. H., & Hernquist, L. 1996, ApJS, 105, 19 (KWH)
Katz, N., Weinberg, D. H., Hernquist, L., & Miralda-Escudé, J. 1996, ApJ, 457, L57 (KWHM)
Kauffmann, G., & Charlot, S. 1994, ApJ, 430, L97

Klypin, A., Borgani, S., Holtzman, J., & Primack, J. 1995 *ApJ*, 444, 1

Lacey, C., & Cole, S. 1994, *MNRAS*, 271, 676

Lanzetta, K. M., & Bowen, D. 1990, *ApJ*, 357, 321

Lanzetta, K. M., Webb, J. K., & Barcons, X. 1996, *ApJ*, 456, L17

Ma, C. 1996, in press, (astro-ph 9605198)

Ma, C., & Bertschinger, E. 1994, *ApJ*, 434, L5

Miralda-Escudé, J., Cen, R. Y., Ostriker, J. P., & Rauch, M. 1996, *ApJ*, in press

Mo, H. J., Jing, Y. P., & White, S. D. M. 1996, *MNRAS*, submitted, (astro-ph 9602052)

Mo, H. J., & Miralda-Escudé, J. 1994, *ApJ*, 430, L25

Mo, H. J., & Miralda-Escudé, J. 1996, *ApJ*, (astro-ph 9605138)

Navarro, J., & Steinmetz, M. 1996, *ApJ*, submitted (astro-ph 9605043)

Petitjean, P., Mücke, J. P., & Kates, R. 1995, *A&A*, in press

Press, W. H., & Schechter, P. L. 1974, *ApJ*, 187, 425

Quinn, T. R., Katz, N., & Efstathiou, G. 1996, *MNRAS*, 278, L49

Stadel, J., Katz, N., Weinberg, D. H., & Hernquist, L. 1996, in preparation

Steidel, C. C., Dickinson, M., & Persson, S. E. 1994, *ApJ*, 437, L75

Storrie-Lombardi, L. J., Irwin, M. J., & McMahon, R. G. 1996, *MNRAS*, in publication, (astro-ph 9608146)

Storrie-Lombardi, L. J., McMahon, R. G., Irwin, M. J., & Hazard, C. 1994, *ApJ*, 427, L13

Thoul, A. A. & Weinberg, D. H. 1996, *ApJ*, 465, 608

Weinberg, D. H., Hernquist, L., & Katz, N. 1996, *ApJ*, in press

Wolfe, A. M. 1988, in *QSO Absorption Lines: Probing the Universe*, ed. J. C. Blades, D. A. Turnshek, & C. A. Norman (Cambridge: Cambridge Univ. Press), 297

Wolfe, A. M., Lanzetta, K. M., Foltz, C. B., & Chaffee, F. H. 1995, *ApJ*, 454, 698

Wolfe, A. M., Turnshek, Lanzetta, K. M., & Lu, L. 1993, *ApJ*, 385, 151

Wolfe, A. M., Xiao, M. F., Tytler, D., Vogt, S. S., Keane, M. J., & Lanzetta, K. M. 1994, *ApJ*, 435, L101

Yanny, B. 1990, *ApJ*, 351, 396

Zhang, Y., Anninos, P., & Norman, M. L. 1995, *ApJ*, 453, L57

Damped Ly α						Lyman Limit					
Calculated			Observed			Calculated			Observed		
z	$n(z)$	F_C	z	$n(z)$		z	$n(z)$	F_C	z	$n(z)$	
2	0.17857	2.05	1.75 ± 0.25	0.14 ± 0.073		2	0.59586	1.74	0.90 ± 0.5	0.65 ± 0.25	
3	0.17411	1.91	2.5 ± 0.5	0.18 ± 0.039		3	0.72439	1.81	2.95 ± 0.6	2.08 ± 0.35	
			3.25 ± 0.25	0.21 ± 0.10							
4	0.19422	2.54	4.1 ± 0.6	0.47 ± 0.17		4	1.00660	2.31	4.15 ± 0.6	3.45 ± 0.95	

Table 2: The incidence $n(z)$ of DLA and Lyman limit absorption for the $\Omega = 1$ CDM model, computed by our calibrated Press-Schechter procedure. Observational values are taken from Storrie-Lombardi et al. (1996) for DLA absorption and from Storrie-Lombardi et al. (1994) for Lyman limit absorption. Also listed is F_C , the correction factor by which the KWHM results for $n(z, 100 \text{ km s}^{-1})$ must be multiplied to obtain the absorption $n(z)$ produced by all halos.